1. Experimental Works for High Pr

1.1 Study of Oscillatory Thermocapillary Flow of High Prandtl Number Fluid

Yasuhiro Kamotani

Case Western Reserve University

STUDY OF OSCILLATORY THERMOCAPILLARY FLOW OF HIGH PRANDTL NUMBER FLUID

Y. Kamotani[1] and S. Yoda[2]

[1]Case Western Reserve University, Cleveland, Ohio 44106, USA
[2]National Space Development Agency of Japan, 2-1-1 Sengen, Tsukuba, 305-8505, Japan

Oscillatory thermocapillary flow is investigated for high Prandtl number fluids. The main objective is to delineate the physical mechanism of oscillations. The investigation is done experimentally as well as numerically. Some model problems are analyzed numerically to identify some important features of oscillations. The model predictions are compared with the experimental information whenever possible. The oscillation process is shown to be very much affected by the flow in the hot corner and by the thermal boundary layer along the hot wall. It is shown experimentally that it takes some time before the oscillations can be detected when the imposed temperature difference is very close to the critical value but they appear very quickly just above the onset point.

1. INTRODUCTION

Much attention has been given lately to thermocapillary flow in the so-called half zone (or liquid bridge) configuration, in which a liquid column is suspended between two differentially heated metal rods, because of its similarity to the floating-zone crystal growth technique. Many experiments have been performed in the past with high Prandtl fluids because it is easier to perform thermocapillary flow experiments with those fluids due to their insensitivity to surface contamination. Those experiments have shown that thermocapillary flow in the half-zone configuration becomes oscillatory. However, despite the fact that much experimental information is available, the cause of oscillations is not yet fully understood. The main objective of the present work is to clarify the cause of oscillations in the half-zone and similar configurations for high Prandtl number fluids.

In order to understand the oscillation mechanism, it is important to know the basic flow field. Kamotani and Ostrach [1] analyzed the basic flow and temperature fields in the half-zone configuration for high Prandtl number fluids. They have derived the scaling laws for various flow variables and have shown that the flow is mainly driven in a relatively small region near the hot wall, called the hot corner. The oscillation process is also observed to start from the hot corner. Based on the information on the basic flow field and also on the experimentally known conditions for the onset of oscillations, Kamotani and Ostrach [1] postulated an oscillation mechanism involving dynamic free surface deformation (free surface deformation caused by fluid motion). Kamotani and Ostrach [2,3] also analyzed the oscillation phenomena in other configurations and proposed similar oscillation mechanisms involving dynamic free surface deformation. The present work is an extension of those studies and is intended to clarify the postulated model further.

If dynamic free surface deformation were important in the oscillation mechanism, as postulated, the best way to prove the model would be to control the deformation experimentally and study its effect on the onset of oscillations. However, this direct approach

is not feasible technically, so we must rely on other ways to prove the postulate. One way is to simulate the oscillation phenomenon numerically. Since it is very difficult to include the dynamic free surface deformation in the analysis of actual oscillatory flow in the float-zone configuration, we analyze some model problems in order to clarify some important features of oscillation mechanism. As mentioned above, much experimental information is available mainly concerning the conditions for the onset of oscillations. However, some of the data are contradictory or the data tend to scatter considerably, which is one of the main reasons for the lack of our clear understanding of the oscillation mechanism. We want to clarify the reasons for some misleading trends. We also investigate some important aspects of oscillations that have not been investigated before in order to give some new light into the oscillation mechanism.

2. NUMERICAL INVESTIGATION OF BASIC OSCILLATION PROCESS

2.1. Basic Steady Flow Field

The half-zone configuration and the coordinate system adopted herein are illustrated in Fig. 1. The important dimensionless parameters for steady thermocapillary flow in this configuration in the absence of gravity with flat free surface are known to be: Marangoni number $Ma = \sigma_T \Delta T L/\mu\alpha$, Prandtl number $Pr = \nu/\alpha$, and aspect ratio $Ar = L/2R$, where σ_T is the temperature coefficient of surface tension, ΔT is the imposed temperature difference between the hot and cold walls ($= T_H - T_C$), L is the length of liquid column, R is the radius, μ is the dynamic viscosity of the fluid, ν is the kinematic viscosity, and α is the thermal diffusivity. The Reynolds number of the flow, $R\sigma$, is related to Ma and Pr as $R\sigma = Ma/Pr$.

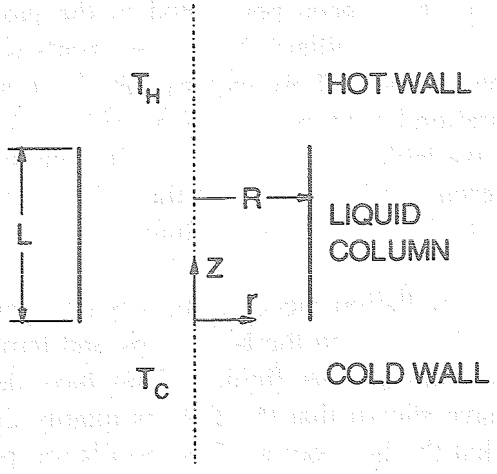

Fig. 1 Half-zone configuration

One important feature of thermocapillary flow of high Pr fluid at high Ma is the existence of a hot corner where the flow driving force is concentrated. Typical streamline and isotherm patterns, which are computed numerically, are presented in Fig. 2 for steady thermocapillary flow at a high Ma. Since the flow is axisymmetric, the flow and temperature fields in one radial (r-z) plane are shown. A thermal boundary layer is clearly recognizable along the hot wall. Because of the thermal boundary layer, a large temperature gradient is generated along the free surface near the hot wall. Since the surface temperature gradient

determines the thermocapillary driving force, large driving force exists in that small region near the hot wall, called the hot corner, and the driving force is relatively small outside the corner. Therefore, the overall flow is mainly driven in the hot corner (Kamotani and Ostrach [1]) so that the center of unicellular motion is located near the hot wall as seen in Fig. 2.

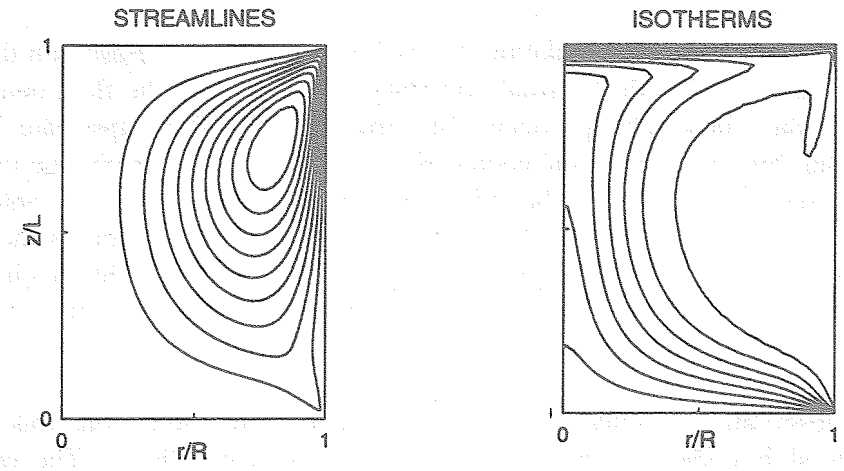

Fig. 2 Computed streamlines and isotherms for Ma = 1.1 x 10^5, Ar = 0.7 and Pr = 50

2.2. Time Scale of Oscillation Process

During oscillations, the whole flow field is known to change cyclically. Since the flow is driven mainly in the hot corner, the driving force there must also be altered periodically. The only way to change the hot corner temperature distribution, thus the driving force, is to change the thermal boundary layer thickness along the hot wall. The thermal boundary layer is closely related to the heat transfer at the hot wall. In order to see how the heat transfer is distributed over the hot wall surface, the dimensionless heat flux at the wall ($\partial T/\partial z\,|_{z=L}$ ($L/\Delta T$)) multiplied by r/R (to take into account area change in the radial direction) is shown in Fig. 3. Since the flow is squeezed into the relatively small hot corner, the shear stress at the hot wall is the main retarding force for the flow. For that reason the dimensionless shear stress at the hot wall ($\partial v/\partial z\,|_{z=L}$ ($L/\sigma_T\,\Delta T$)$(L/R)^2$), multiplied by r/R, is also shown in Fig. 3.

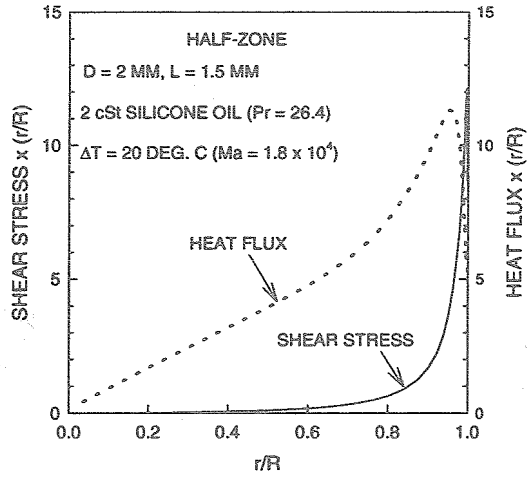

Fig. 3 Distributions of shear stress and heat flux along hot wall

As the figure shows, the whole hot surface is contributing to the overall heat transfer. That suggests that during oscillations the boundary layer over the entire hot surface must be altered. In contrast, the shear stress is much more concentrated in the hot corner, which means that the flow retarding force is adjusted relatively quickly after a change in the driving force (and thus the flow field) in the hot corner, namely the flow field is quasi-steady.

From the above result one can make the following observation. Based on the concept of boundary layer, we know that the thermal boundary changes when the flow near it is altered and that the boundary layer change occurs starting from the flow upstream region. The upstream region in this case is near the centerline (near r = 0). After a change in the velocity field in the bulk region, the thermal boundary begins to change from the centerline region toward the free surface region (near r = R). Therefore, since the hot corner is located near the free surface, it takes some time before the driving force and the flow field are changed. From this one can infer that the period of oscillations should scale with the time scale associated with the thermal boundary layer.

The above observation is checked in the numerical simulation. For this purpose, we disturb the thermal boundary layer and determine its recovery time. The recovery time represents the time scale of the boundary layer and is compared with available experimentally observed oscillation frequency. Numerically, we first obtain a steady solution for the conditions that are known to be close to the onset of oscillations, and then we suddenly increase Ma by a small amount (10%) and monitor the subsequent variation of the total heat transfer rate (Nusselt number) at the hot wall.

In our ground-based experiments we often use 2-centistokes silicone oil. To minimize buoyancy, we usually use 2-mm dia. liquid columns. We have accumulated much experimental information for those conditions, so the computations are done for those conditions for comparison. To cover a much wider range of Ma, without introducing buoyancy, we also analyze the conditions of the microgravity experiments by Monti et al. [4]. Two computational results are presented in Fig. 4. As the figure shows, the total heat transfer rate increases when Ma is increased and eventually reaches a plateau. Since the heat transfer rate approaches the plateau asymptotically, one cannot cleanly determine the time to get there. Instead, we determine the time constant from the time it takes to reach 90% of the final value, as shown in Fig. 4.

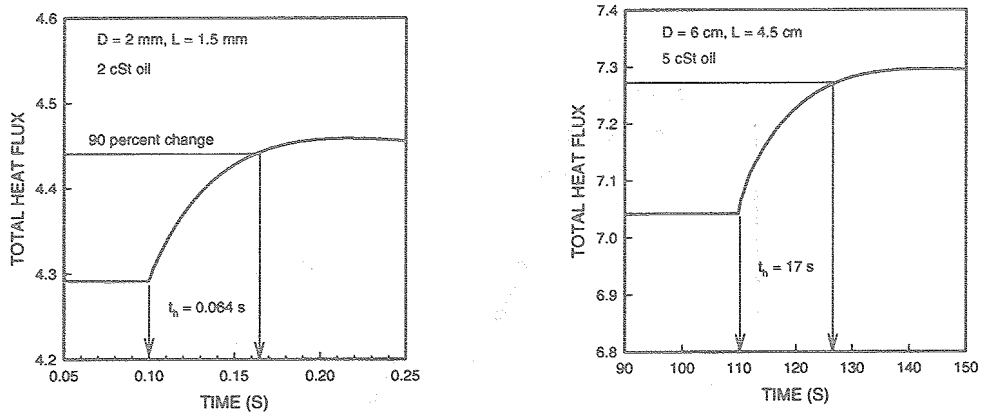

Fig. 4 Variation of total heat flux at hot wall after a sudden increase in Ma

The boundary layer time constant, t_h, is compared with observed oscillation period, t_p, in Table 1. To show that t_h scales with t_p, the ratio t_p/t_h is computed. As the table shows, the ratio is indeed nearly constant in those tests.

Table 1 Comparison of boundary layer time constant and oscillation period

D (cm)	L (cm)	Fluid	t_h (s)	t_p (s)	t_p/t_h
0.20	0.15	2 cSt	0.064	0.33	5.1
0.20	0.10	2 cSt	0.044	0.23	5.2
3.00	6.00	5 cSt	6.0	31.3	5.2
4.50	3.40	5 cSt	11.5	47.6	4.1
4.50	4.50	5 cSt	13.5	71.4	5.3
6.00	4.50	5 cSt	17.0	83.3	4.9

In order to show that the above time scale, t_h, is the time scale for the thermal boundary layer, we use the result of the scaling analysis performed by Kamotani and Ostrach [1]. They have shown that there exists only one velocity scale, U_0, in the problem. Based on [1], U_0 scales as $(\sigma_T \Delta T/\mu)Ma^{-1/7}$. From boundary layer theory, the time scale for the boundary scales with the time of convection along the hot wall, namely $R/U_0 \sim (RL/\alpha)Ma^{-6/7}$. Then, if the computed time constant, t_h, scales with the boundary layer time scale, the ratio $t_h/(R/U_0)$ would be constant. The ratio is shown in Fig. 5. The figure shows that the ratio is indeed nearly constant over a wide range of Ma.

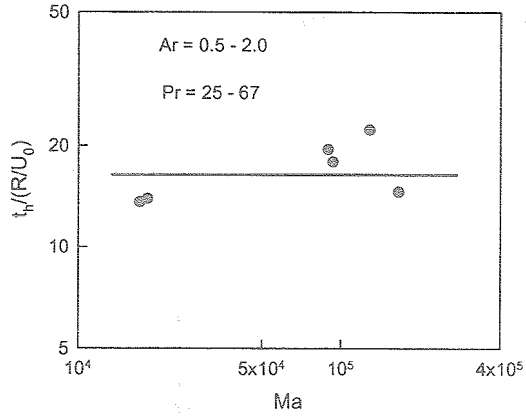

Fig. 5 Comparison of boundary time constant and convection time

From the above discussion one can conclude that the period of oscillation scales with the time scale of the thermal boundary layer along the hot wall. Since the thermal boundary layer is closely related to the hot corner, the above conclusion shows the importance of the hot corner in the oscillation mechanism.

2.3. Flow Adjustment Process

Next we discuss how the flow adjusts itself after it is disturbed. It is important to understand this adjustment process before we investigate the cause of oscillation process, as shown below. For that purpose we disturb the flow in the following way in the numerical

simulation. After a steady flow is obtained, the value of Ma is increased by 30% for a certain time. After that, Ma is decreased to the original value. Various dimensionless quantities are monitored in the subsequent time. One example is shown in Fig. 5, where the dimensionless total heat transfer rate (Nusselt number) at the hot wall is monitored after the disturbance. As the figure shows, the response to the disturbance is periodic with the amplitude decaying with time.

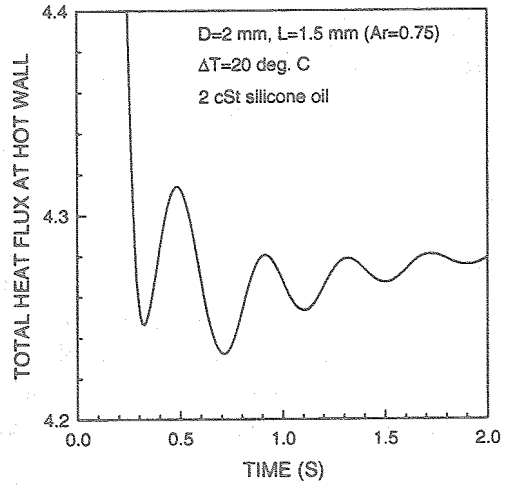

Fig. 6 Variation of total heat flux at hot wall after disturbance

Since the flow adjustment is periodic, it is useful to see how other quantities are varying with time during that period. We consider two quantities: the maximum stream function, which represents the strength of the overall flow, and the total shear at the hot wall, which represents the flow retarding force as discussed above. Figure 7 shows the phase relations among those quantities for the conditions of Fig. 6.

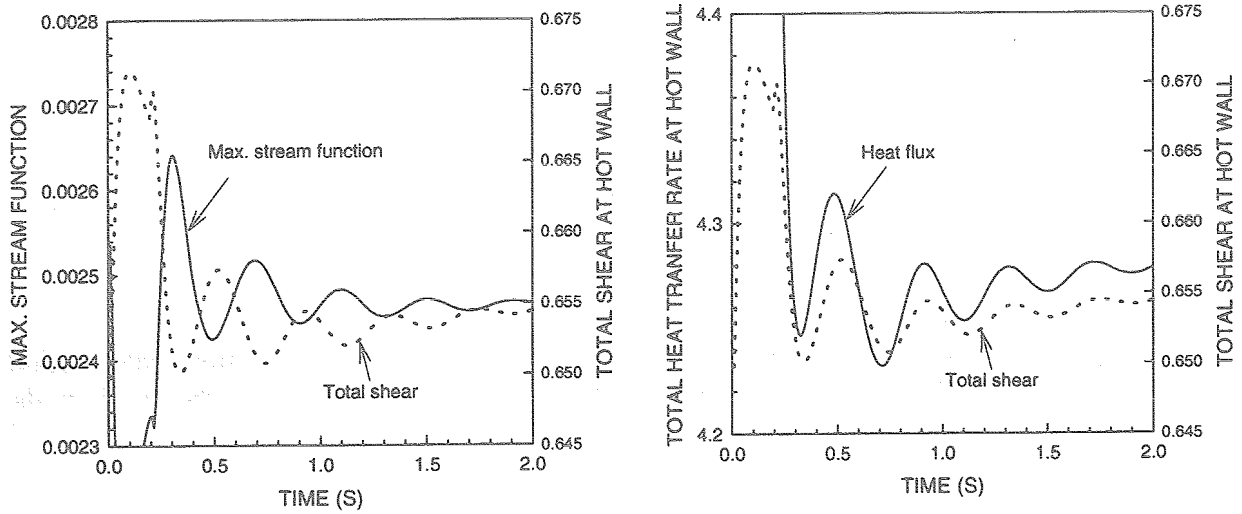

Fig. 7 Variations of dimensionless maximum stream function and total shear at hot wall relative to that of heat flux

The maximum stream function variation and the total shear variation at the hot wall are nearly out-of-phase. This means that when the shear is large (small), the bulk flow is weak

(strong), which makes sense because the shear is the main retarding force. Since the flow is viscous-dominated, the wall effect is felt very quickly by the bulk flow. The total shear variation and the heat flux variation are nearly in-phase. This means that when the thermal boundary layer is thin (which increases the heat transfer), the hot corner is narrower, which increases the wall shear effect. Putting that information together, we get the following picture. When the bulk flow becomes strong, the thermal boundary layer becomes thinner after some time, which increases the wall shear and slows the bulk flow. The opposite happens when the bulk flow becomes weak. This mechanism simply tries to bring the whole situation back to the original state. In order to oscillate, the adjustment process must overshoot and undershoot the original state (non-linear effect). In the process shown in Figs. 6 and 7, the non-linear effect comes from the inertia forces, but the inertia forces are not strong enough to sustain oscillations. We will discuss this in the next section.

2.4. Effect of Inertia Forces in Oscillation Mechanism

As discussed above, the inertia forces make the flow adjustment oscillatory. Since the inertia forces become more important with increasing Reynolds number ($R\sigma$), we analyze the flow adjustment process after the disturbance described above for one of the conditions in the microgravity experiment by Monti et al. [4]. One result is shown in Fig. 8, where $R\sigma$ is 2.2×10^3. At this $R\sigma$ it becomes extremely time-consuming to obtain grid-independent solution, so the result shown in Fig. 8 is not exactly grid-independent. Nevertheless, at this very large $R\sigma$, the oscillatory process seems to sustain itself. The oscillation period in Fig. 8 is 125 seconds, compared to the measured oscillation period of 83.3.seconds (see Table 1). In Fig. 6 the oscillation period is 0.39 seconds compared to the measured period of 0.33 seconds. The fact that the computed periods of oscillations associated with the inertia forces are in reasonable agreement with the measured ones suggests that the inertia forces play some role in the oscillation process. However, it is important to note that the inertia forces by themselves cannot generate oscillations generally, because we observe oscillations experimentally in small liquid bridges where $R\sigma$ is relatively small. The requirement that we need an extra feature to explain the oscillations makes this problem very complex. In the next Chapter, we discuss the situation where the extra feature is given by a relatively simple phenomenon.

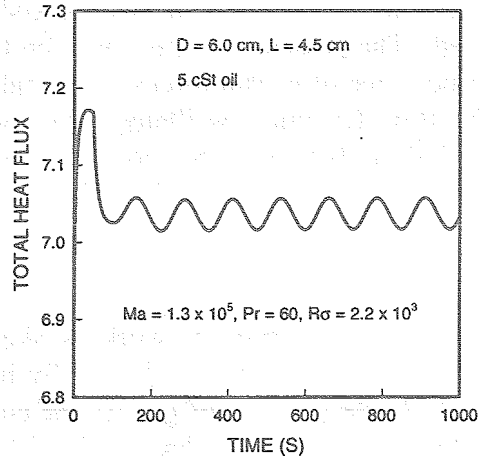

Fig. 8 Oscillations at high Reynolds number.

3. A NUMERICAL STUDY OF THERMOCAPILLARY CONVECTION IN TWO-DIMENSIONAL LIQUID BRIDGES WITH CURVED FREE SURFACES

3.1. Introduction

Thermocapillary flow in the so-called half-zone (or liquid-bridge) configuration is known to become oscillatory under certain conditions. High Prandtl number liquids were used in most of past thermocapillary flow experiments because of their relative insensitivity to surface contamination (e.g. [5,6]). It is known experimentally that the onset of oscillatory thermocapillary flow of high Prandtl fluids depends very much on the liquid bridge shape [7, 8], but the reason for the strong shape effect is not yet well understood. Although the oscillation phenomenon in liquid bridges of unit-order Prandtl number fluids with flat free surfaces has been analyzed as a type of hydrodynamic instability in the past (e.g. Wanschura et al. [9]), no such study exists for high Prandtl number (> 15) fluids with curved free surfaces.

In the present work, steady and oscillatory thermocapillary convection in liquid bridges of a high Prandtl number fluid is investigated numerically. Although the oscillation phenomenon is known to be three-dimensional generally, an accurate three-dimensional simulation of oscillatory flow of a high Prandtl number fluid with a curved free surface is computationally extremely time-consuming and is beyond the scope of the present study. Instead, a two-dimensional version of the half-zone is considered in order to simplify the computation and to gain some physical insight into the oscillation phenomenon with curved free surfaces. In the past, combined thermocapillary and buoyancy convection has been investigated numerically for two-dimensional liquid bridges [10] and for axisymmetric flow in cylindrical bridges [11], both with curved free surfaces. No oscillatory flow was found without buoyancy in those studies. Also related to the present work, Peltier and Biringen [12] numerically investigated oscillatory thermocapillary flow in two-dimensional rectangular open containers with flat free surfaces for Prandtl number = 6.78. No oscillations were found when the container aspect ratio (length/depth ratio) was smaller than 2.3. The present two-dimensional simulation does not include buoyancy and our range of interest of Ar is near unity, but the flow is shown to become oscillatory under some conditions. The present result also shows strong dependency of the onset of oscillations on the free surface shape. Some implications of the present results to the experimentally observed oscillation phenomenon in cylindrical bridges are discussed. The present paper is based on the thesis by Gupta [13]. In Chapter 2 we discussed the importance of inertia forces. The subject is explored also in this chapter. It is shown that the flow becomes oscillatory even when the inertia forces are negligible and also without including dynamic free surface deformation. This work shows that the subject of oscillatory thermocapillary flow in high Pr fluid is a complex one.

3.2. Problem Formulation

The configuration investigated in the present work is sketched in Fig. 9. A two-dimensional liquid bridge is formed between two differentially heated plates. The two free surfaces are either flat or curved. In the absence of gravity the curved surface shape is a part of a circle. The coordinate system adopted in this chapter is defined also in Fig. 9.

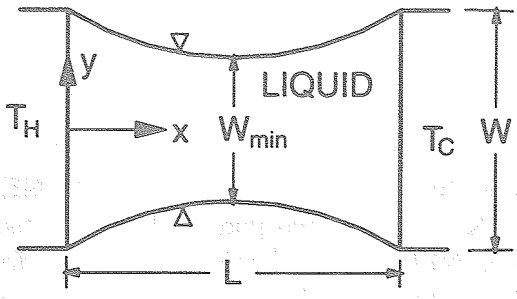

Fig. 9 Two-dimensional liquid bridge with curved free surfaces

The following assumptions are made in the present analysis: (i) The flow is laminar and incompressible. (ii) The fluid properties are constant except for the surface tension which is considered to vary linearly with temperature. (iii) The heat loss from the liquid free surfaces is negligible.

The continuity, momentum and energy equations can be expressed in dimensionless form as:

$$\frac{\partial u}{\partial x}+\frac{\partial v}{\partial y}=0$$

$$\frac{\partial u}{\partial t}+u\frac{\partial u}{\partial x}+v\frac{\partial u}{\partial y}=-\frac{\partial p}{\partial x}+\frac{1}{ArR\sigma}\left(\frac{\partial^2 u}{\partial x^2}+Ar^2\frac{\partial^2 u}{\partial y^2}\right)$$

$$\frac{\partial v}{\partial t}+u\frac{\partial v}{\partial x}+v\frac{\partial v}{\partial y}=-Ar^2\frac{\partial p}{\partial y}+\frac{1}{ArR\sigma}\left(\frac{\partial^2 v}{\partial x^2}+Ar^2\frac{\partial^2 v}{\partial y^2}\right)$$

$$\frac{\partial T}{\partial t}+u\frac{\partial T}{\partial x}+v\frac{\partial T}{\partial y}=\frac{1}{ArMa}\left(\frac{\partial^2 T}{\partial x^2}+Ar^2\frac{\partial^2 T}{\partial y^2}\right)$$

The x-coordinate, y-coordinate, velocities, pressure, and time in the above equations are non-dimensionalized by L, W, $\sigma_T\Delta T/\mu$, $\rho(\sigma_T\Delta T/\mu)^2$, and $\mu L/\sigma_T\Delta T$, respectively. Temperature is made dimensionless as $(T-T_C)/\Delta T$. The boundary conditions at the walls are: $u = v = 0$ and $T = 1$ at $x = 0$. $u = v = T = 0$ at $x = 1$. Along each free surface we have: negligible heat loss condition ($\partial T/\partial n = 0$) and tangential stress balance ($\partial u_s/\partial n=\partial T/\partial s$).

From the above formulation one sees that the important dimensionless parameters in the present problem are Marangoni number ($Ma = \sigma_T\Delta TL/\mu\alpha$), surface tension Reynolds number ($R\sigma = \sigma_T\Delta TL/\mu\nu$), and aspect ratio ($Ar = H/W$). Ma and $R\sigma$ are related through Prandtl number ($Pr = \nu/\alpha$) as $Ma = R\sigma\ Pr$. In addition, the static liquid free surface shape is represented by Ar and width ratio ($Dr = W_{min}/W$). The fluid motion also deforms the free surface but the dynamic free surface deformation relative to the liquid bridge dimension is generally much less than unity [8], so the surface deformation by fluid motion is neglected in the present analysis. A more discussion on the effect of dynamic free surface deformation will be given later in conjunction with the oscillation mechanism.

The parametric ranges investigated in the present analysis correspond mostly to the conditions of our past experiments, for comparison purpose. The physical properties are those of 2 centistokes silicone oil ($Pr = 27$). The liquid bridge width is 3 mm and the imposed temperature difference (ΔT) ranges from 1 to 30 °C. Thus, $R\sigma$ ranges from 3.2×10^2

to 1.9×10^3 and Ma from 8.6×10^3 to 5.2×10^4. Ar ranges from 0.6 to 1.4, and Dr from 0.4 to 1.

3.3. Numerical Scheme

A commercial computational fluid dynamics package called NEKTON is used for the present numerical analysis. NEKTON is a two-part package consisting of a preprocessor, GeoMesh, and a main module, NEKTON. GeoMesh is used for geometry and mesh generation purposes. NEKTON is based on the Spectral Element Method. The dependent variables are expanded in terms of N^{th}-order tensor-product Lagrangian interpolants. The semi-discrete algebraic equations are generated based on the governing equations using weighted-residual techniques. Those equations are solved by either direct or indirect iterative solution techniques based on the conjugate gradient method. For transient simulations, NEKTON employs both explicit and implicit time-integration techniques, and the solution is updated to the next time level using various combinations of multi-step and multi-stage schemes. The convective terms are treated implicitly or explicitly, using a third order Adams-Bashforth multi-step scheme or a fourth-order Runge-Kutta multi-stage scheme. The diffusion terms are treated implicitly using a first- or second-order backward differential multi-step scheme. Further details regarding NEKTON can be found in [14]. NEKTON has been used in past numerical studies of various subjects including thermocapillary convection (e.g. Bullister et al. [15])

For all steady and unsteady simulations, the calculations are started with a 120-element second-order grid and then the order is increased to three. A direct-coupled solver is employed as the solution technique for all cases. Since the direct-coupled solver is used, the convection term is treated implicitly, so there is no time step restriction for stability. However, it is selected as 0.01 seconds to accurately capture the transient characteristics of the thermocapillary convection phenomenon. The numerical scheme is under-relaxed by specifying relaxation parameter as 0.3 as it is found to be diverging in some cases where the relaxation parameter value exceeds 0.3. The solution process is controlled by the following convergence criteria: (i) The maximum relative change between two successive iterations for the velocity and scalar fields is specified as 10^{-5}. (ii) The residual tolerance for velocity and pressure values is specified as 10^{-5}. A more detailed description of the present numerical procedure is given in [13].

3.4. Results and Discussion

3.4.1. Choice of numerical grid

The numerical grid adopted herein is discussed first. The initial grid is chosen as a uniform grid of 80 quadrilateral elements of second order. Then, the grid is refined by monitoring various important quantities of the flow (the maximum stream function, streamline and isotherm patterns, surface velocity and temperature distributions, maximum surface velocity near the hot wall, and, in the case of unsteady flow, temperature variations with time at various points). Table 2 summarizes typical grid study for steady and unsteady flows with highly curved free surfaces (Dr=0.4). More detailed comparisons of other quantities with various grids are given in [13]. Based on those grid studies, the third-order 120-element non-uniform grid is used for Dr=0.4, increasing to sixth-order 120-element for

flat free surfaces, in the present study. The chosen grid for Dr=0.4 is shown in Fig. 10. The grid has finer resolutions along the free surfaces and also along the hot and cold walls because of thermal boundary layers in those regions.

Table 2 Effect of numerical grid on steady and oscillatory flows (Ar=1, Dr=0.4, Ma=2.6x10^4)

No. of Elements	Order	Ψ_{max}	$u_{s,max}$
80	2	0.00117	0.0206
108	2	0.00112	0.0212
120	2	0.00101	0.0205
120	3	0.00102	0.0196
120	4	0.00103	0.0196

(a) Steady convection

No. of Elements	Order	Surface Temp. at Point 1	Surface Temp. at Point 2
120	2	0.753	0.616
120	3	0.782	0.638
120	4	0.773	0.643

(b) Oscillatory convection, free surface temperature at a specific time (point 1 at x=0.3, and point 2 at x=0.7)

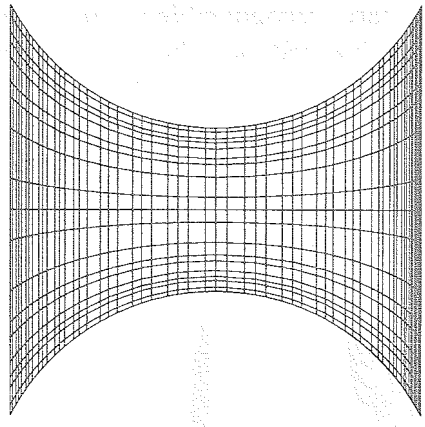

Fig. 10 Computational mesh for Dr = 0.4 and Ar = 1.

3.4.2. Steady thermocapillary convection

In order to analyze the effect of width ratio (Dr) on the steady flow field, it is varied from 0.4 to 1, while keeping Ar and Ma constant (Ar=1 and Ma=1.7 x 10^4). Some computed streamline patterns are presented in Fig. 11, which shows that the flow is symmetrical with respect to the middle plane parallel to the x-axis. For Dr > 0.6, the flow is unicellular on each side of the middle plane, with the cell center located near the corner of the hot wall and the free surface. The flow along the free surface toward the cold wall is called the surface flow and the interior flow toward the hot wall is called the return flow herein. When Dr becomes

below 0.6, the single-cell structure changes to a two-cell flow structure with the formation of a second cell near x = 0.5 (called the bridge neck region herein). The secondary cell near the neck is observed experimentally in an axisymmetric liquid bridge. However, in the case of the cylindrical configuration, the cross-sectional area at the neck is proportional to the square of the neck radius, so the flow passage near the neck is more strongly affected by Dr than in the present two-dimensional configuration. For example, we observe the secondary cell experimentally even near Dr = 0.8 for Ar = 1.

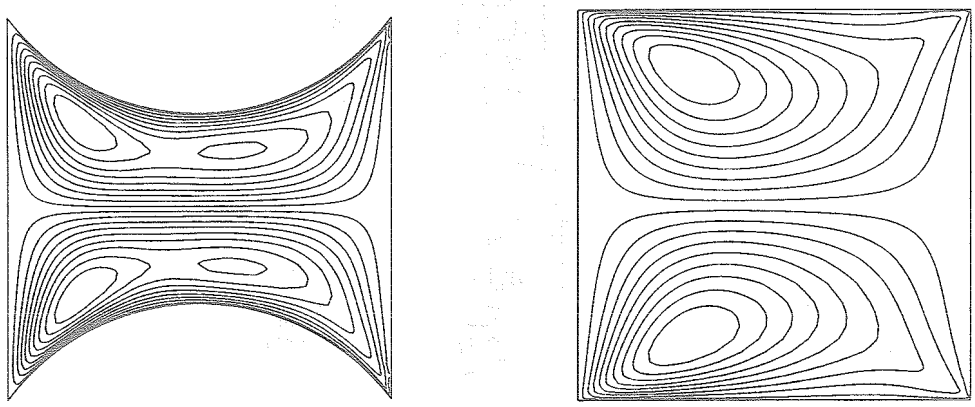

(a) Dr = 0.5 (b) Dr = 1.0

Fig. 11 Effect of Dr on streamline pattern (Ar = 1, Ma = 1.7×10^4)

The isotherm patterns corresponding to the conditions of Fig. 11 are presented in Fig. 12. In all cases a thermal boundary is clearly recognizable along the hot wall. As the flow along the hot wall turns at the corner of the hot wall and the free surface, called the hot corner, the fluid is mixed with the return flow and the temperature decreases quickly. Also, the isotherms bunch up in a small corner of the cold wall and the free surface, called the cold corner, due to the convection of hot fluid along the free surface to the region close to the cold wall.

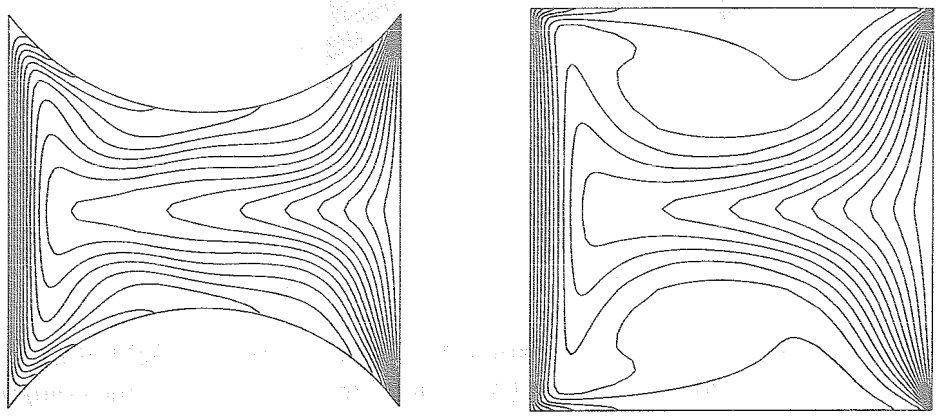

(a) Dr = 0.5 (b) Dr = 1.0

Fig. 12 Effect of Dr on isotherm pattern (Ar = 1, Ma = 1.7×10^4)

Those hot and cold corner phenomena are some of the important features of thermocapillary flow of high Pr fluid at large Ma [1]. The free surface temperature is relatively uniform in the region away from those corners when Dr is near unity. As the free surface becomes more concave, the convection in the hot and cold corners becomes weaker due to increasingly narrow flow passages in those corners, so the isotherms bunch up less in those corners, although the corner regions are still recognizable.

One important feature of thermocapillary flow of high Pr fluid in a container of unit-order Ar is that the flow is mainly driven in the hot corner at large Ma (e.g. Kamotani and Ostrach [1]). That is why the center of main flow cell is located near the hot wall in Fig. 11(b) even when the free surface is curved. When the surface is concave, the flow cell tends to be more elongated along the free surface due to slightly more spread-out driving force distribution and also due to increased length of the free surface. As the neck region becomes too narrow, the elongated cell is pinched near the neck to create an additional closed cell.

Since the flow is mainly driven in the relatively small hot corner, it is very much affected by the viscous forces even when the Reynolds number is large [1]. The values of dimensionless maximum stream function, computed with and without the inertia forces in the momentum equations, are presented in Fig. 13 at a Reynolds number which is near the onset of oscillations to be discussed later. Ψ_{max} increases with increasing Dr as the overall flow passage increases. As seen in the figure, although the inertia forces are not negligible generally, Ψ_{max} is mainly determined by the viscous forces. When Dr is below about 0.6, the flow becomes viscous-dominated as the overall flow passage is more squeezed. The fact that the flow is strongly affected by the viscous forces will become important when we analyze the oscillation mechanism later.

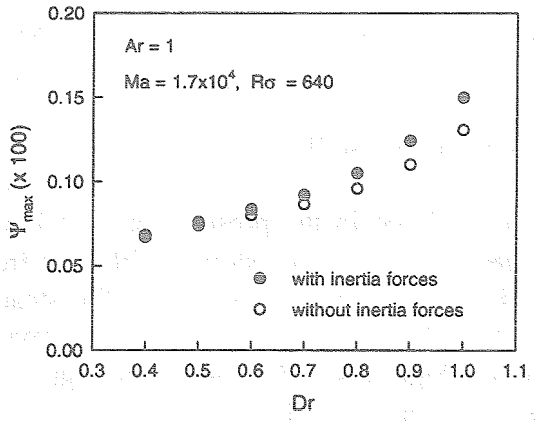

Fig. 13 Effect of Dr on maximum stream function with and without inertia forces (Ar = 1, Ma = 1.1 x 10^4, Rσ = 390)

The effect of aspect ratio on the streamline pattern is shown in Fig. 14 for Dr=0.4. For Ar > 0.6, the two-cell structure is observed, which changes to the unicellular structure for Ar ≤ 0.6. The transition from the one-cell to the two-cell flow structure can be again attributed to the decreased flow passage at the neck region. As the liquid bridge becomes longer (larger Ar), the overall cell becomes more elongated so that it becomes more susceptible to pinching near the neck. This means that the two-cell structure appears at larger value of Dr when Ar becomes larger.

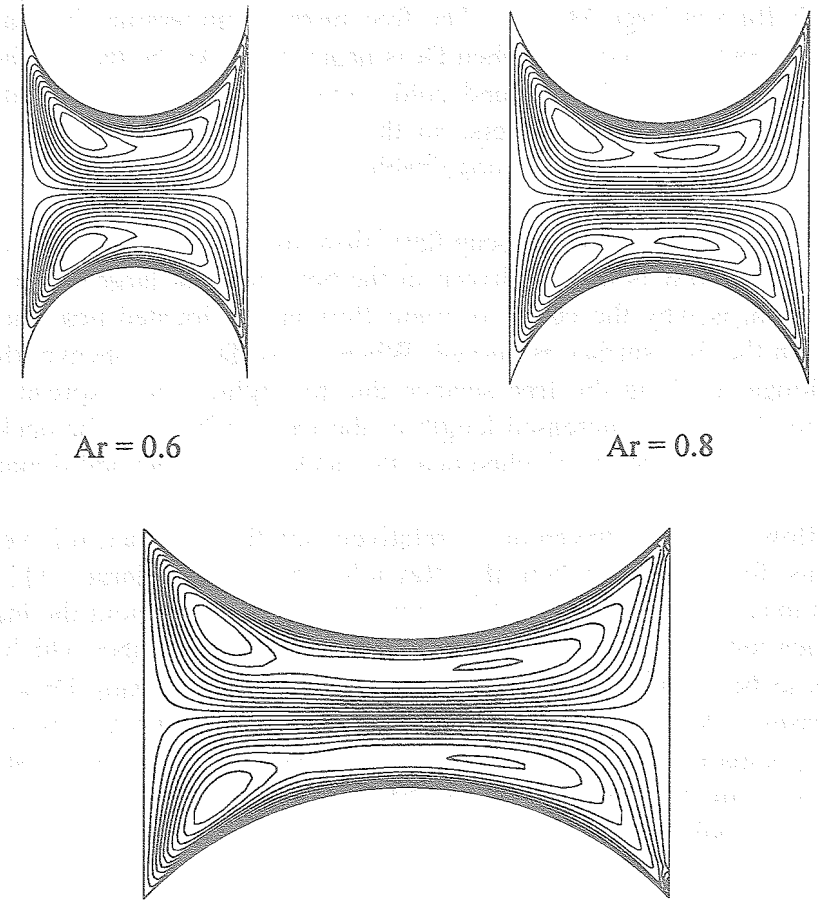

Fig. 14 Effect of Ar on streamline pattern (Dr = 0.4, Ma/Ar = 1.8×10^4)

3.4.3. Critical temperature difference for oscillatory thermocapillary convection

For the parametric ranges considered in the present study, it is observed that the flow always remains quasi-steady when ΔT is increased slowly with time from a small value. It is found, however, that when a finite disturbance is given to the steady flow, the flow can become oscillatory beyond a critical temperature difference. To provide a finite disturbance to the steady flow, the procedure adopted is as follows. For a given case, ΔT is increased from 1°C to a desired value and a steady solution is obtained. After the steady solution is obtained, one of the free surfaces is made shear free for a fixed time (0.5 seconds) by changing its boundary condition. The choice of 0.5 seconds is made to ensure that the total flow domain gets considerably disturbed. After providing the finite disturbance for 0.5 seconds to the flow, the original shear boundary condition is restored and the subsequent behavior of the flow is observed.

Two examples of the unsteady calculation are shown in Fig. 15 for Dr=0.4 and Ar=1. The disturbance is provided to the steady flow at ΔT = 8 and 12 °C. For convenient comparison with available experimental information, we use dimensional ΔT here. For the ΔT = 8 °C case, the fluid temperature becomes steady after a few oscillations of diminishing amplitude (Fig. 15a). However, for the ΔT = 12 °C case, the velocity and temperature

oscillations persist after the disturbance (Fig. 15b). It means that the critical ΔT for the onset of oscillations (ΔT_{cr}) lies between 8 and 12 °C. It will be shown later that ΔT_{cr} for this case is 10.7 °C. In order to find ΔT_{cr}, ΔT is decreased slowly from a value at which the oscillations are found to occur to a value at which they just disappear (below the aforementioned computational tolerance limit). The decrement in ΔT is carried out in steps of 0.1 °C, and it is made sure at each ΔT that the oscillations become quasi-steady.

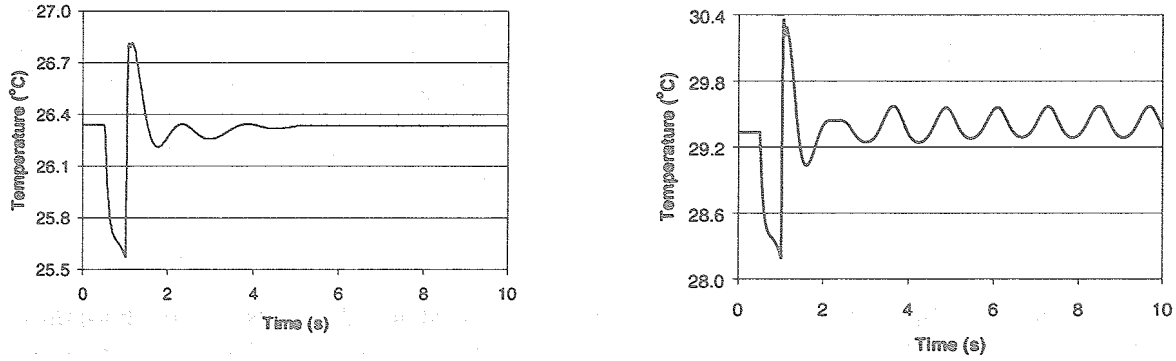

Fig. 15 Temperature variation after initial disturbance (Dr = 0.4, Ar = 1, surface temperature at x = 0.3)

Figure 16 shows the dependence of ΔT_{cr} on Dr for Ar=1. The corresponding value of Ma is also given in the figure. The curve in Fig. 16 consists of two separate branches, which correspond to the fat bridge (Dr larger about 0.65) and the slender bridge (Dr smaller than about 0.55), respectively. In the slender bridge branch, ΔT_{cr} increases with increasing Dr. On the other side, ΔT_{cr} decreases with increasing Dr. There is a gap in between where oscillations are not realized for ΔT up to 30 °C. Those two branches correspond to the aforementioned two basic flow structures, the unicellular flow structure for the fat bridge branch and the two-cell structure for the slender bridge branch.

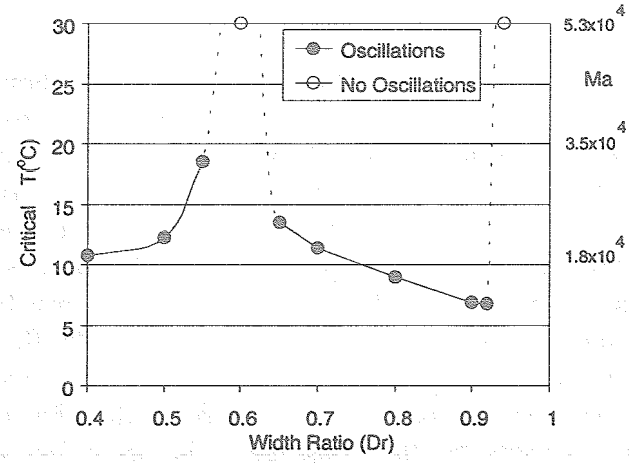

Fig. 16 Dependency of ΔT_{cr} on Dr for Ar = 1

The above trend is qualitatively similar to the experimentally observed trend for the cylindrical half-zone configuration. It is known experimentally that there are two branches in the ΔT_{cr}-Dr curve for a given Ar and that there exists a narrow gap in between where ΔT_{cr} increases sharply [7,8]. It is mentioned in [8] that each branch is associated with the one- or the two-cell basic flow structure, as found in the present analysis. The gap region is near Dr = 0.6 in the present two-dimensional analysis with Ar = 1, while experimentally it is around Dr = 0.8-0.9 for Ar = 1 [7]. Although it is not shown here, the present analysis shows that the gap region moves to higher Dr range as Ar is increased [13], which is also known experimentally, because the transition from the one- to two-cell structure occurs at a larger value of Dr with increasing Ar, as discussed above in conjunction with Fig. 14. In addition, the range of ΔT_{cr} in Fig. 16 is nearly the same as the experimentally observed range for 3 mm diameter cylindrical liquid bridges of 2 centistokes silicone oil (7 – 20 °C) [8]. The computed oscillation frequency near ΔT_{cr} of Fig. 15 is about 1 Hz, while the measured frequency in the above experiment is about 2 Hz.

3.4.4. Physical mechanisms of oscillations

One important objective of the present work is to delineate the physical mechanism of oscillations. The fact that there are two branches in Fig. 16 suggests that there exist two different oscillation processes. It is found that one important difference is the role of inertia forces. It can be shown that in the case of fat bridges the oscillations disappear if we remove the inertia terms in the momentum equations, while they persist in the slender bridges after the removal [13]. Therefore, the oscillation mechanism must include the inertia forces for the fat bridges but not for the slender bridges. That finding is consistent with the fact that the basic flow is very much dominated by the viscous forces in the slender bridges near the onset of oscillations but the inertia forces are small but not completely negligible in the fat bridges, as shown in Fig. 5. Although there exist two different oscillation processes, the key feature of oscillation mechanism remains the same, as seen below. The key feature is associated with the hot corner, where the flow is mainly driven in the case of high Pr fluids. As described in [1] in detail, the overall flow activity is determined by the extent of the hot corner for a given ΔT: strong flow when the hot corner is extended and weak flow when it shrinks. The oscillatory thermocapillary flow in shallow rectangular containers investigated numerically by Peltier and Biringen [12] is explained also by the change in the hot corner extent.

We discuss first the oscillation mechanism for the slender bridge branch (Dr $\leq$ 0.55 for Ar = 1). A typical oscillation cycle is shown in Figs. 17 and 18, where the streamline and isotherm patterns are shown at four different times in one cycle of oscillations (they are equally spaced in time). As seen in the figure, the flow is no longer symmetric with respect to the x-axis during oscillations and the secondary cells near the cold wall are varying with time prominently. Since the inertia forces are not important, the viscous-dominated flow and the temperature field must interact non-linearly through the shear stress boundary condition at the free surface to cause the oscillations. By examining closely the flow patterns as well as the surface velocity and temperature distributions at various times, one oscillation cycle is found to proceed as follows. As discussed earlier, the basic flow has the two-cell structure because the neck region constricts the flow passage. The secondary cell near the neck is called the cold cell herein. As seen in Fig. 17(a), the cold cell in the upper half is strong when that in the lower half is weak. The strong cold cell widens the passage in the neck region for the flow in the upper half. As a result, more cold fluid is brought to the hot corner

in the upper half, as the isotherms near the hot wall in Fig. 18(b) indicate (cold isotherms are directed towards the hot corner), which eventually shrinks the hot corner.

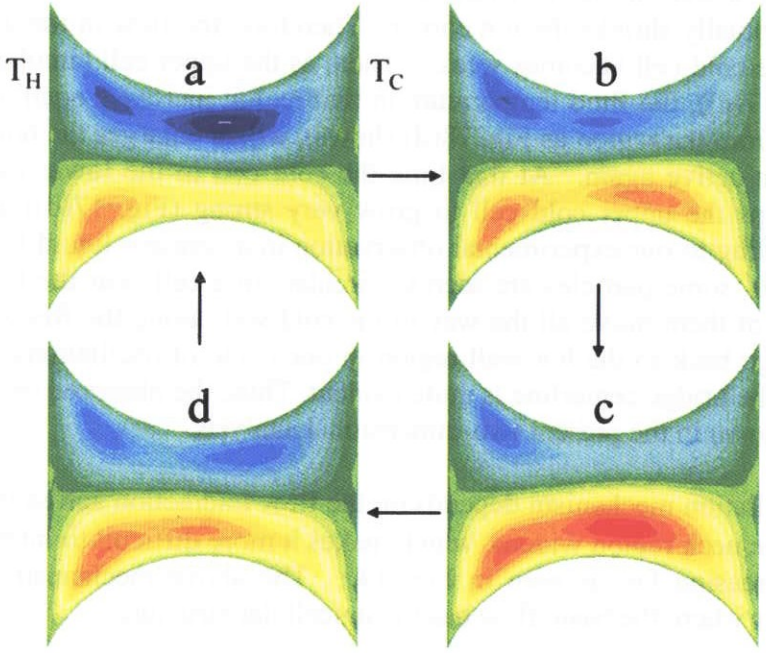

Fig. 17 Variation of streamline pattern in one cycle of oscillations (equally spaced in time) for Dr = 0.4, Ar = 1, Ma = 2.1 x 10^4

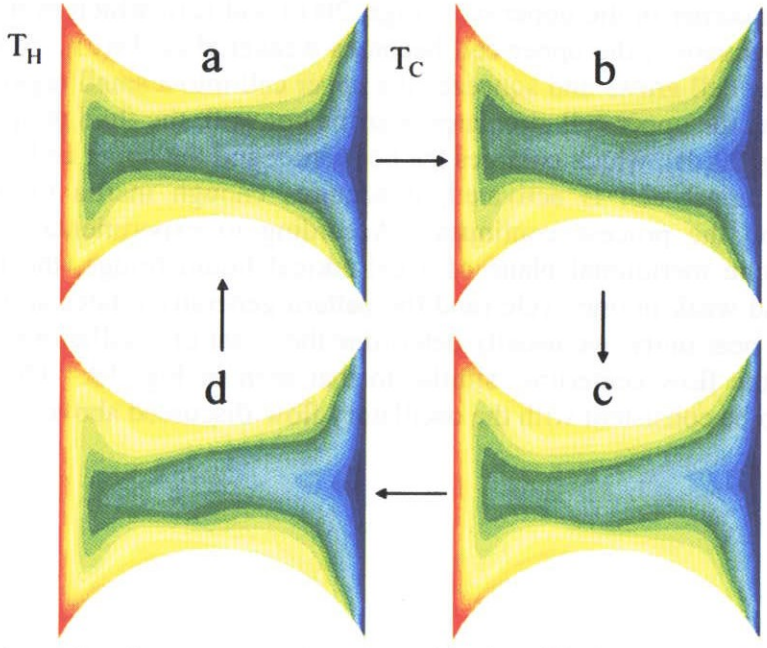

Fig. 18 Variation of isotherm pattern in one cycle of oscillations (equally spaced in time) for Dr = 0.4, Ar = 1, Ma = 2.1 x 10^4

As discussed earlier, the basic flow has the two-cell structure because the neck region constricts the flow passage. The secondary cell near the neck is called the cold cell herein. As seen in Fig. 17(a), the cold cell in the upper half is strong when that in the lower half is weak. The strong cold cell widens the passage in the neck region for the flow in the upper half. As a result, more cold fluid is brought to the hot corner in the upper half, as the isotherms near the hot wall in Fig. 18(b) indicate (cold isotherms are directed towards the hot corner), which eventually shrinks the hot corner. Therefore, the flow in the upper half slows (Fig. 17(b)) and the cold cell becomes weak. Then, as the upper cell circulates mainly near the hot wall (Fig. 17(c)), the fluid temperature in that region increases again (cold isotherms are directed away from the region as Fig. 18(d) shows), which enlarges the hot corner and the upper cell becomes active again. At that time the cold cell in the lower half is becoming weaker, which helps the upper cold cell to grow very strong (Fig. 17(d)) and the process continues. According to our experimental observation in a concave liquid bridge near Ar=1 with tracer particles, some particles are seen to circulate in a cell near the hot corner at one time. Then, some of them move all the way to the cold wall along the free surface, activate the cold cell, and go back to the hot wall region in one cycle of oscillations. A strong flow interaction across the bridge centerline is quite evident. Thus, the observed oscillation process is similar to that shown in the present two-dimensional analysis.

The above oscillation mechanism depends on the flow interaction across the middle plane. As Dr increases, the neck region widens, which makes it more difficult to interact so that ΔT_{cr} increases with increasing Dr, as seen in Fig. 14. The above mechanism does not work beyond a certain Dr where the basic flow has the unicellular structure.

A typical oscillation cycle for a fat bridge is shown in Figs. 19 and 20. There exists only one main cell in each half of the bridge. Each cell becomes alternately large and small in one cycle. When the upper cell grows larger, it overshoots the equilibrium state (the state corresponding to the steady-state solution) due to the effect of inertia forces and squeezes the lower cell. The upper cell is strongest in Fig. 19(a). The strong cell eventually brings cold fluid towards the hot corner in the upper half (Figs. 20(b) and (c)), which eventually shrinks the hot corner. Consequently, the upper cell becomes weaker (Fig. 19(c)). When the upper cell shrinks, the lower cell grows and squeezes the upper cell into a small region near the hot wall (Fig. 19(d)). As the upper cell circulates near the hot wall, the fluid temperature in that region increases (Fig. 20(d)), which enlarges the hot corner and the upper cell becomes active again. When the upper cell is activated, it acquires enough inertia to grow past the equilibrium state and the process continues. According to experimental observation of oscillatory flow in one meridional plane of a cylindrical liquid bridge, the flow becomes alternately strong and weak in one cycle (and the pattern generally rotates around the center axis).[4] When Ar is near unity, we usually determine the onset of oscillations by detecting a slight wobbling of the flow centerline, similar to that seen in Fig. 19. The experimental information seems to be consistent with the oscillatory flow discussed above.

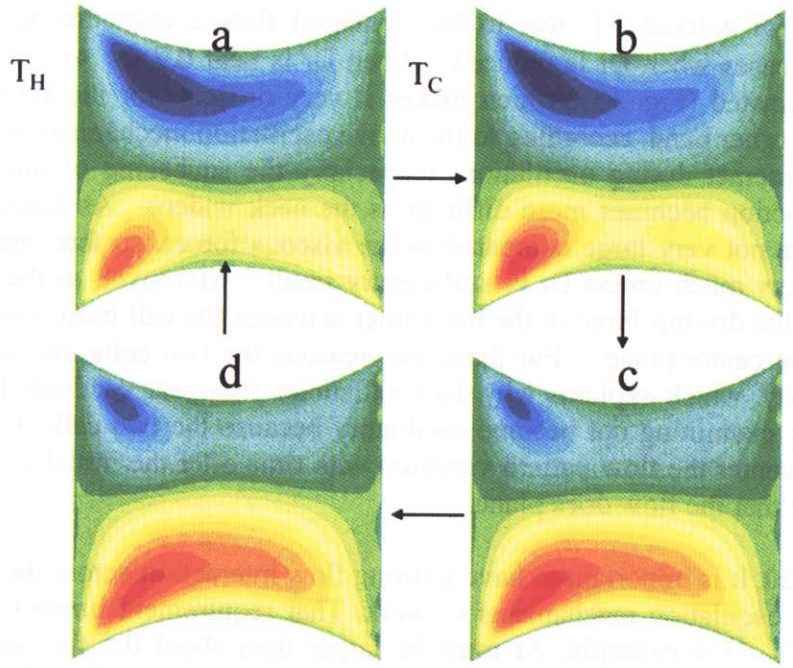

Fig. 19 Variation of streamline pattern in one cycle of oscillations (equally spaced in time) for Dr = 0.7, Ar = 1, Ma = 2.1 x 10^4

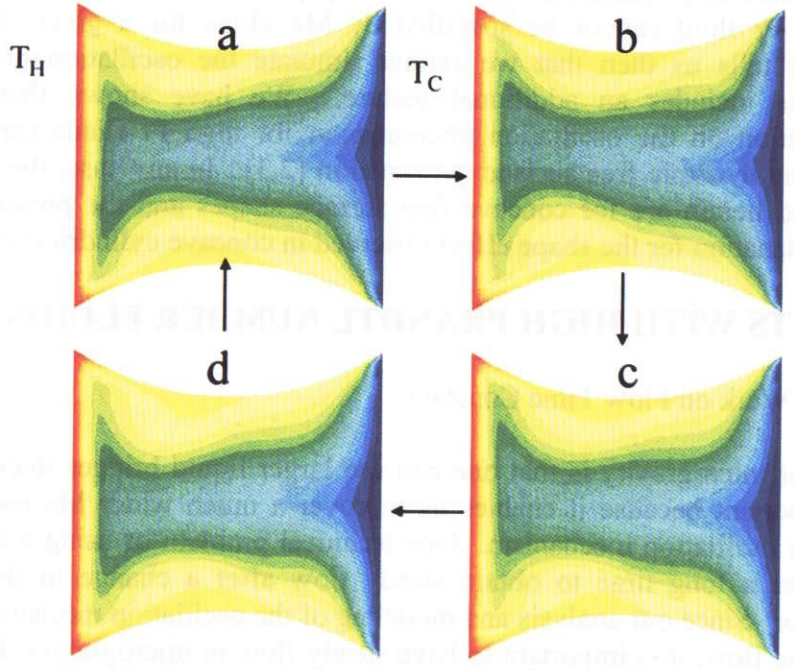

Fig. 20 Variation of isotherm pattern in one cycle of oscillations (equally spaced in time) for Dr = 0.7, Ar = 1, Ma = 2.1 x 10^4

In the case of a fat bridge, the bridge neck has two different effects. As Dr is reduced, the overall flow slows for a fixed ΔT, due to the increased flow constriction near the neck. Therefore, ΔT_{cr} increases when Dr is reduced. When Dr is near 0.7 for Ar = 1, the flow is almost viscous-dominated (Fig. 13), which makes it very difficult for the flow to become oscillatory. On the other hand, according to the above oscillation mechanism, it is important that the two cells interact during oscillations (especially the squeezing of one cell by the other) but the interaction becomes more difficult as the neck widens. As discussed earlier, the inertia forces are not very large compared to the viscous forces, so that one cell cannot squeeze the other very much unless Dr is sufficiently small. Moreover, as the free surface becomes more flat, the driving force in the hot corner activates the cell more toward the cold wall, less toward the center plane. For those two reasons the two cells interact much less when Dr is near unity, which explains why the oscillations disappear suddenly beyond Dr = 0.92 in Fig. 16. By examining not become oscillatory because the two cells do not interact strongly across the center the flow pattern variation with time after the initial disturbance for Dr = 0.95, it is clear that the flow does plane.

As seen in Fig. 20, it is important to have a strong flow interaction across the center plane for the present two oscillation mechanisms to work. That requirement limits the applicable ranges of Ar and Dr. For example, Ar must be larger than about 0.5 for nearly flat free surfaces. Within those ranges, the predicted oscillatory flow patterns appear to agree, at least qualitatively, with the experimentally observed flows in cylindrical bridges. No oscillations were found in the present analysis when the free surfaces are nearly flat. In that case it may be necessary to perform three-dimensional simulations to obtain oscillations. However, we have investigated the oscillation phenomenon in cylindrical bridges with nearly flat free surfaces for many years (e.g. Kamotani and Ostrach [1]) and showed that the onset of oscillations for high Pr fluid cannot be specified by Ma alone for a given Ar and Pr. Dimensional analysis tells us then that we cannot simulate the oscillation phenomenon accurately unless one includes an additional feature. We have shown that available experimental information on the oscillation phenomenon for high Pr fluids can be made consistent by including dynamic free surface deformation [2,3]. In any case, the oscillation mechanisms discussed herein are for concave free surface shapes and the present analysis seems to offer an explanation for the shape effect observed in concave cylindrical bridges.

4. EXPERIMENTS WITH HIGH PRANDTL NUMBER FLUIDS

4.1. Experimental Work on Flow Time Constant

One advantage of microgravity is that one can use larger liquid bridges than in normal gravity. This is important because it enables us to cover a much wider Ma range, which could help clarify the oscillation mechanism. One technical problem of using a large liquid bridge is that it takes a long time to obtain steady flow after a change in the imposed temperature difference. Since our analysis and modeling of the oscillation mechanism will be limited to steady basic flow, it is important to have steady flow in microgravity. It is known that if we use the Marangoni number to specify the onset of oscillations, the difference between the critical Marangoni number determined in normal gravity tests with small liquid bridges and that determined in microgravity tests with large liquid bridges is as large as one order of magnitude [8]. Then, an important question arises: is it possible to explain that much difference by the fact that the flow is not actually steady in large liquid bridges used in microgravity? For that reason we investigate some time constants associated with the

thermocapillary flow in a liquid bridge and their relation to the time for the oscillations to appear.

For this experiment we use the test apparatus used in the Surface Tension Driven Convection Experiment (STDCE). The test chamber is a circular dish with a cylindrical heater placed along the centerline, as shown in Fig. 21. The fluid is 2 cSt silicone oil. The test chamber diameter is 1.2 cm. From a comparison of onset conditions of oscillations in microgravity and those in normal gravity, we know that buoyancy does not have appreciable effect in the case of the 1.2 cm chamber [3]. Although buoyancy is nearly negligible, the chamber is not very small compared to liquid bridges in normal gravity, which makes it easier to measure some flow time constants. Another important reason we use this apparatus in the present work, instead of our half-zone apparatus, is that it is designed to heat up the heater very quickly so that, when we investigate the fluid temperature variation after a change in the heater input, we can neglect the heater warm up time. In contrast, for our liquid bridge apparatus the warm-up time of heater element is usually longer than that of the fluid. Numerical analysis is also performed to supplement the experiment.

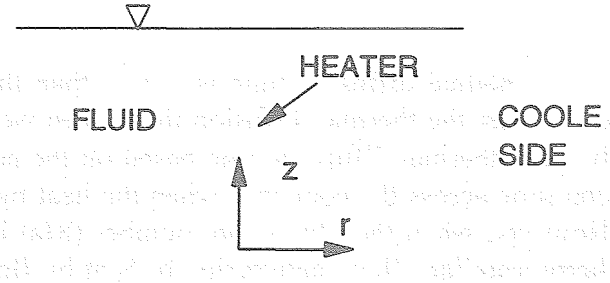

Fig. 21 Test chamber for STDCE experiment

In order to check the accuracy of the numerical simulation, we compare the predicted fluid temperature variation with the measured temperature variation after a step change in the heater power input. The fluid temperature is measured by thermistor probe which is located at r/R = 0.5 but whose height is variable. In Fig. 22 we compare them at two points and good agreement is shown. The numerical simulation assumes zero warm-up time for the heater. The fact that it predicts the fluid temperature variation well suggests that the heater warm-up time is indeed small.

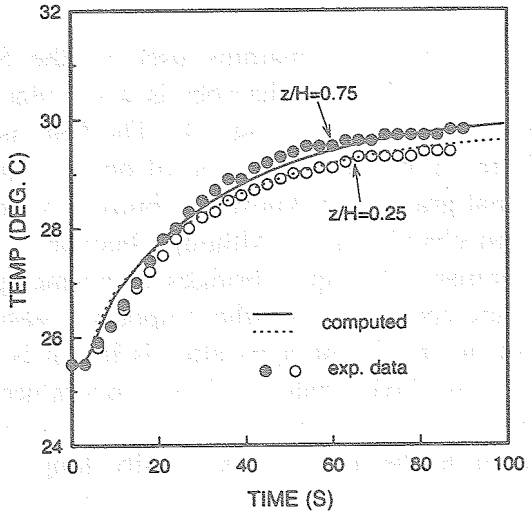

Fig. 22 Comparison of computed and measured fluid temperature variation with time after a step change in heater input

For high Pr fluids, the thermal diffusion time is longer than the viscous diffusion time. Therefore, we have to consider the thermal diffusion time when we estimate the time for the flow to become steady. The thermal diffusion time based on the container radius, R^2/α, is a measure of the diffusion time across the container when the heat transfer through the fluid is mainly conduction. However, when the Marangoni number (Ma) is much larger than unity, as in the oscillatory thermocapillary flow, convection of heat by fluid flow is very important and spreads the heat quickly over the whole flow field, so the fluid heats up relatively quickly. In Fig. 23 we compare the warm-up time in the conduction-dominant case with that due to convection, based on the numerical simulation for the 1.2 cm chamber. Under steady condition the total heat flux from the heater is balanced by the total heat removed at the cold

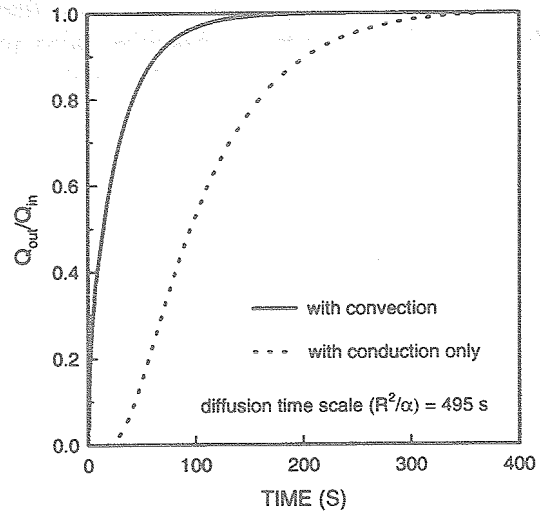

Fig. 23 Computed variation of heat flux ratio after a step change in heater heat flux

wall, so the ratio of those fluxes is used as a measure of flow steadiness in Fig. 23. The overall diffusion time (R^2/α) is estimated to be 495 seconds. In the case of conduction heat transfer the warm-up time (~ 400 s) is comparable with that estimate. With convection, the warm-up time is reduced to about 200 s. The difference becomes larger when a larger system is used in microgravity as Ma increases. Since the diffusion time increases with the square of the fluid dimension, it becomes large quickly with increasing size. For example, it is about 3.5 hours when the dimension is 3 cm for 2 cSt fluid, but it dose not take such a long time for the flow field to become steady.

After knowing the time constants of the basic flow, it is interesting to check how long it will take before we observe oscillations if we step-change the heater input from zero to a certain value and to compare the waiting period with the time constants. In reality we do not change the heat flux so abruptly when we want to identify the onset of oscillations accurately, but the test gives us information about the worst case. The result is summarized in Table 3.

Table 3 Effect of step change in heater input on time to observe onset of oscillations

Q_{HEATER} (W)*	ΔT	time to oscillations (s)	oscillation pattern**
0.95	25.3	no oscillations	
1.00	26.3	273	P & R
1.05	27.9	201	P & R
1.10	28.7	133	P
1.15	29.8	113	P & R
1.20	31.0	93	P & R

(* $Q_{heater,critical}$ = 0.97 W, **P = pulsating pattern, R = rotating pattern)

A few conclusions can be drawn. First, if the abrupt change is to a heat flux below the critical heat flux, no oscillations will appear, in other words, the abrupt change will not cause the flow to become oscillatory. Therefore, we can heat up the fluid quickly to a state just below the critical state (assuming that we know a priori the critical state, at least approximately). Second, it will take a long time before oscillations appear if the change is to just above the critical temperature difference, but the waiting time will decrease quickly if the change is to an increasingly larger value above the critical. The oscillation pattern observed in our microgravity tests was a pulsating pattern near the onset of oscillations and it changed to a rotating pattern at slightly higher ΔT. In the present test we observe a combination of pulsating and rotating pattern. Based on the information from this worst case study, one can infer the following. If, in a test, we increase the heater temperature gradually from the initial uniform temperature state and eventually observe the onset of oscillations after the time that is about the time constant of convection (~ 200 s), the error in determining the critical temperature difference will be only about 10 %. The error will become smaller if we heat more slowly so that it takes longer time to observe the onset of oscillations, but the improvement may not be significant knowing the experimental error and repeatability in the measurement. So the convection time gives us a good measure as to how fast we can heat up the fluid. On the other hand, if we want to study a succession of oscillation patterns in the post critical regime, we need to be more careful about the heating rate. According to Table 3, the waiting time becomes very large as we get close to the critical point. Therefore, we investigate near the critical point in details next.

For this test chamber we know that the heat input to the heater corresponding to the critical temperature difference is Q = 0.97 W, when we keep T_C at 25 °C. We first heat the fluid at Q_0 = 0.96 W and obtain steady flow. Then we increase Q to a value above the critical value and measure the time it takes to observe the onset of oscillations. We repeat the test for various Q, always starting from Q_0. The result is shown in Fig. 24. As seen in the figure, the time to observe oscillations is rather large very near the critical temperature difference, about 25 minutes. The time is much larger than the aforementioned time scales. During that time the temperatures of heater, cold wall and air are all measured to be steady. The result tells us

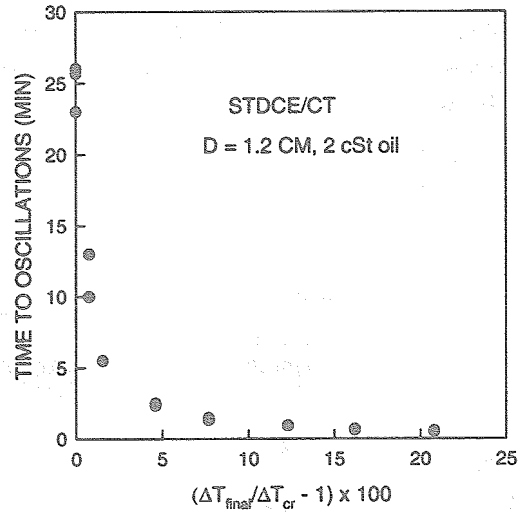

Fig. 24 Time to observe oscillations as a function of $\Delta T/\Delta T_{cr}$

that the oscillation phenomenon is a very slowly growing process at or just above the critical point. We are investigating this long waiting period further. It turns out that this long waiting period very near the onset of oscillations is a strong function of T_C. We are investigating whether any external disturbances can change this waiting period. In practice we may not wait that long near Q = 0.97 W (unless we know a priori that the oscillations will appear eventually as in the present work), so we do not measure the critical temperature difference correctly. But with increasing Q, the waiting time goes down exponentially. Therefore, if we are carefully investigating the onset conditions around the critical state, the heat rate does not cause much error.

One main conclusion from this study is that we cannot explain the aforementioned one order of magnitude difference in the critical Ma by the fluid heating up rate alone.

REFERENCES

[1] Kamotani, Y. and Ostrach, S.: "Theoretical Analysis of Thermocapillary Flow in Cylindrical Columns of High Prandtl Number Fluids," Journal of Heat Transfer, Vol.120 (1998), pp. 758-764.

[2] Kamotani, Y., Ostrach, S., and Masud, J.: "Oscillatory Thermocapillary flows in Open Cylindrical Containers Induced by CO_2 Laser Heating," International Journal of Heat and Mass Transfer Vol. 42 (1998), pp. 555-564.
[3] Kamotani, Y., Ostrach, S., and Masud, J.: "Microgravity Experiments and Analysis of Oscillatory Thermocapillary Flows in Cylindrical Containers," Journal of Fluid Mechanics, Vol. 410 (2000), pp. 211-233.
[4] Monti, R., Albanese, C., Carotenuto, L., Castagnolo, D., and Evangelista, G.: "An Investigation on the Onset of Oscillatiory Marangoni Flow," Advances in Space Research, Vol. 16 (1995), pp. 87-94.
[5] Preisser, F., Schwabe, D., and Scharmann, A.: "Steady and Oscillatory Thermocapillary Convection in Liquid Columns with Free Cylindrical Surface," Journal of Fluid Mechanics, Vol. 126 (1983), pp. 545-567.
[6] Velten, R., Schwabe, D., and Scharmann, A.: "The Periodic Instability of Thermocapillary Convection in Cylindrical Liquid Bridges," Physics of Fluids A, Vol. 3 (1991), pp. 267-279.
[7] Hu, W. R., Shu, J. Z., Zhou, R., and Tang, Z. M.: "Influence of Liquid Bridge Volume on the Onset of Oscillation in Floating Zone Convection, I. Experiments," Journal of Crystal Growth, Vol. 142 (1994), pp. 379-384.
[8] Masud, J., Kamotani, Y., and Ostrach, S.: "Oscillatory Thermocapillary Flow in Cylindrical Columns of High Prandtl Number Fluids," Journal of Thermophysics and Heat Transfer, Vol. 11 (1997), pp. 105-111.
[9] Wanschura, M., Shevtsova, V. M., Kuhlmann, H. C., and Rath, H. J.: "Convective Instability Mechanisms in Thermocapillary Liquid Bridges," Physics of Fluids, Vol.7 (1995), 912-925.
[10] Tang, Z. M. and Hu, W. R.: "Influence of Liquid Bridge Volume on the Onset of Oscillation in Floating Zone Convection, II. Numerical Simulation," Journal of Crystal Growth, Vol. 142 (1994), pp. 385-391.
[11] Shevtsova, V. M. and Legros, J. C.: "Oscillatory Convective Motion in Deformed Liquid Bridges," Physics of Fluids, Vol. 10 (1998), pp. 1621-1634.
[12] Peltier, L. J. and Biringen, S.: "Time-Dependent Thermocapillary Convection in a Rectangular Cavity: Numerical Results for a Moderate Prandtl Number Fluid," Journal of Fluid Mechanics, Vol. 257 (1993), pp. 339-357.
[13] Gupta, S., "A Numerical Study of Thermocapillary Convection in Two-Dimensional Liquid Bridges for a High Prandtl Number Liquid," M. S. Thesis, Department f Mechanical and Aerospace Engineering, Case Western Reserve University, 1999.
[14] NEKTON Version 3.1.1. Users Manual, Fluent Inc., 1996.
[15] Bullister, E. T., Ho, L. W., Ronquist, E. M., and Patera, A. T., "Computational Environment for Microgravity Materials Processing Simulations," Final Report on NASA Contract NAS3-26132, 1991.